

A combined analysis of cluster mass estimates from strong lensing, X-ray measurement and the universal density profile

Xiang-Ping Wu

Beijing Astronomical Observatory and National Astronomical Observatories, Chinese Academy of Sciences, Beijing 100012, China

Accepted 2000 February 22. Received 1999 December 2; in original form 1999 May 4

ABSTRACT

We present a combined analysis of mass estimates in the central cores of galaxy clusters from the strong lensing, the X-ray measurements and the universal density profile (NFW). Special attention is paid to the questions (1) whether the previously claimed mass discrepancy between the strong lensing and X-ray measurements is associated with the presence of cooling/non-cooling flows, (2) whether the cusped NFW density model can provide a consistent cluster mass with the strong lensing result and (3) whether a non-zero cosmological constant can be of any help to reducing the strong lensing – X-ray mass ratios. We analyse a sample of 26 arc-like images among 21 clusters, the X-ray data of which are available in archive. The X-ray and NFW cluster masses are obtained by assuming that the intracluster gas is isothermal and in hydrostatic equilibrium with the underlying gravitational potential of the clusters.

A statistical comparison of these three mass estimates reveals that the mass discrepancies for all the events are well within a factor of 2, if X-ray measurement uncertainties are included. In particular, we confirm the result of Allen that the larger mass discrepancy is only detected in the intermediate cooling, especially non-cooling flow clusters, thus attributing the mass discrepancy to the local dynamical activities in the central regions. We show that the NFW profile yields a consistent cluster mass with the conventional X-ray measurement, which is interpreted as the consequence of the common working hypothesis behind the two methods. Any difference between these two models must occur at even smaller radii (e.g. within the arc-like images) or at large radii. It appears that the introduction of the cusped density profile as the dark matter distribution of clusters cannot raise the cluster masses enclosed within arc-like images. Finally, a non-zero cosmological constant is able to moderately reduce the mass ratios of m_{lens} to m_{xray} . These results, together with the excellent agreement between the X-ray, optical and weak lensing determined cluster masses on scales greater than the X-ray core sizes found in the early work, indicate that the mass discrepancy between strong lensing and other methods in the intermediate cooling and non-cooling flow clusters is likely to have arisen from both the oversimplification of lensing model and the inappropriate application of isothermality and equilibrium hypothesis in the central regions of clusters where the local dynamical activities make a non-negligible contribution to both mass estimates.

Key words: clusters: general – dark matter – galaxies: gravitational lensing – X-rays: galaxies.

1 INTRODUCTION

An accurate estimate of the total gravitating masses of clusters of galaxies is crucial for determinations of the mass-to-light ratios M/L and the baryon fractions f_b of clusters, while the latter play a potentially important role in the ‘direct’ measurement of the mean mass density of the

Universe, Ω_M . Four different techniques have been available today to determine the masses of clusters: the optical measurements of distribution and velocity dispersion of cluster galaxies, the X-ray measurements of intracluster gas and its temperature, the gravitationally distorted images of distant galaxies behind clusters, and the numerical simulations

arXiv:astro-ph/0006124v1 9 Jun 2000

of formation and evolution of clusters. Because traditional cluster mass estimators using optical/X-ray observations of galaxies/intracluster gas rely strongly upon the assumption of hydrostatic equilibrium, the gravitational lensing serves as a powerful and efficient tool for both estimating cluster masses and testing the accuracy and reliability of traditional methods. It turns out that there is good agreement between the gravitational lensing, X-ray and optical determined cluster masses on scales larger than the X-ray core radii, within which the X-ray method is likely to underestimate cluster masses by a factor of 2–4 (Wu 1994; Miralda-Escudé & Babul 1995; Wu & Fang 1997; Allen 1998; Wu et al. 1998 and references therein). While a number of mechanisms have been suggested for the reported mass discrepancy (Loeb & Mao 1994; Miralda-Escudé & Babul 1995; Allen 1998), a satisfactory explanation has not yet been achieved. It is generally believed that such a mass discrepancy has probably arisen from either the oversimplification of strong lensing model for the central mass distributions of clusters (Bartelmann & Steinmetz 1996) or the inappropriate application of hydrostatic equilibrium hypothesis in the central regions of clusters (Wu 1994; Wu & Fang 1997).

In this paper we intend to have a close examination of the issue as to whether the reported mass discrepancy is associated with the following three factors: (1) the presence of cooling/non-cooling flows in clusters, (2) the cusped dark matter profile, i.e. the so-called universal density profile (Navarro, Frenk & White 1995; hereafter NFW), as the mass distribution of clusters, and (3) a non-zero cosmological constant (Ω_Λ).

Our reconsideration of the influence of cooling/non-cooling flows on the X-ray mass estimate of clusters is motivated by the pioneering work of Allen (1998), who has demonstrated that there is an excellent agreement between the strong lensing and X-ray determined cluster masses for cooling-flow clusters while the mass discrepancy is only detected among the non-cooling flow ones owing to the significant offsets between the X-ray and lensing centers. If this is the case, the presence or absence of cooling-flows can be used as an indicator of whether or not clusters have reached the state of dynamical relaxation. Meanwhile, the mass discrepancy between the strong lensing and X-ray measurements can be attributed to the local dynamical activities of clusters where the hydrostatic equilibrium assumption becomes invalid. However, such a scenario has been argued recently by Lewis et al. (1999) based on an analysis of 14 CNOC clusters. They have shown that the systematic effects owing to cooling-flows, non-equilibrium systems and temperature gradients on the average ratio of the ‘dynamical’ cluster masses to the X-ray masses do not exceed 15–20 per cent. Therefore, further work is needed to clarify the issue.

The original purpose of this investigation was to study whether the cusped NFW profile as the dark matter distribution of clusters can resolve the discrepancy between the strong lensing and X-ray mass estimates. First, the central singularity in the NFW profile is consistent with the early claim, based on the modeling and statistics of strongly distorted images of background galaxies by massive clusters (Hammer 1991; Wu & Hammer 1993; Grossman & Saha 1994), that dark matter profiles are sharply peaked towards cluster centers. Secondly, except for the small core radius there is a striking similarity between the distribution of in-

tracluster gas tracing the dark halo of the NFW potential and the conventional β model (Makino, Sasaki & Suto 1998). Thirdly, many high-resolution simulations of structure formation have shown that the NFW profile is independent of mass, initial density fluctuation or cosmology (e.g. Cole & Lacey 1996; Navarro, Frenk & White 1997; Eke, Navarro & Frenk 1998). In particular, Makino & Asano (1999) have recently applied the NFW profile to three lensing clusters, A2163, A2218 and RXJ1347, and compared the NFW profile and strong lensing derived cluster masses. Their study indicates that the steeper cusps in the NFW profile can indeed reduce the mass discrepancy between the X-ray and gravitational lensing measurements. On the other hand, the NFW profile can also recover the observed surface number density of cluster galaxies (e.g. Carlberg, Yee & Ellingson 1997), from which one can fix the two free parameters in the NFW profile and then work out the total dynamical masses of the clusters. Using the 14 CNOC distant clusters, Lewis et al. (1999) found no systematic bias between the (NFW) dynamical and X-ray methods. Consequently, the dynamical mass derived from the cusped NFW profile cannot be reconciled with the gravitating mass from strong lensing. This implies that either the NFW profile may not be extrapolated to smaller radii (~ 10 kpc) or the equilibrium hypothesis may break down in the central regions of clusters, provided that the current strong lensing model gives a reliable estimate of the cluster masses enclosed with the arc radii. Alternatively, the giant arc statistics, based on the NFW profile as the underlying gravitational potential and the X-ray measurements of the gas distribution, can marginally reproduce the observed number of giant arcs but requires unreasonably high X-ray temperatures for some clusters (Molikawa et al. 1999). Thus, the detailed modeling of strong lensing including the ‘irregularity’ in the mass distribution of a cluster is once again advocated. Taking these results as a whole, we feel that at least one of the following working hypotheses should be abandoned: (1) a simple estimate of cluster mass from strong lensing, (2) the hydrostatic equilibrium in the central region of a cluster, and (3) the NFW profile as the total mass distribution. In order to stress the point, more examples will be provided in this paper and a systematic comparison among the cluster masses given by the strong lensing, the NFW profile and the X-ray measurements will be made.

Another question we would like to address is how our estimates of the strong lensing and X-ray cluster masses are affected by a non-zero cosmological constant Ω_Λ . This arises because the lensing mass m_{lens} is proportional to $D_d D_s / D_{\text{ds}}$ while the X-ray mass m_{xray} goes as D_d , where D_d , D_s and D_{ds} are the angular diameter distances to the cluster, to the background galaxy, and from the cluster to the galaxy, respectively. As a result, the mass ratio $m_{\text{lens}}/m_{\text{xray}}$ depends on the cosmic density parameter Ω_M and Ω_Λ through D_s/D_{ds} . In particular, $m_{\text{lens}}/m_{\text{xray}}$ becomes smaller in an Ω_Λ dominated universe than in an Ω_M dominated one. This opens a new possibility to reduce the large discrepancy between m_{lens} and m_{xray} . We will compare the lensing and X-ray cluster masses in a flat cosmological model with and without the cosmological constant. Throughout this paper we assume $H_0 = 50 \text{ km s}^{-1} \text{ Mpc}^{-1}$.

2 CLUSTER MASS ESTIMATES

2.1 Strong gravitational lensing

Gravitational lensing furnishes a simple yet efficient way to measure the projected cluster mass along the line of sight. It is believed that a simple spherical lensing model provides rather a good estimate of the projected cluster mass within the position (r_{arc}) of arc-like image, which reads

$$m_{\text{lens}}(< r_{\text{arc}}) = \pi r_{\text{arc}}^2 \Sigma_{\text{crit}}, \quad (1)$$

where $\Sigma_{\text{crit}} = (c^2/4\pi G)(D_s/D_d D_{\text{ds}})$ is the critical surface mass density. The above equation is actually the lensing equation for a cluster lens of spherical mass distribution with a negligibly small alignment parameter for the distant galaxy with respect to r_{arc} . We adopt the value $m_{\text{lens}}(< r_{\text{arc}})$ from the detailed modeling of arclike images where available from literature.

2.2 X-ray measurements

Assuming that the diffuse X-ray emitting gas in a cluster is isothermal and in hydrostatic equilibrium with the underlying gravitational potential of the cluster, we have

$$-\frac{GM(r)}{r^2} = \frac{kT}{\mu m_p} \frac{d \ln n_{\text{gas}}(r)}{dr}, \quad (2)$$

where $M(r)$ is the total cluster mass enclosed within radius r , T and $n_{\text{gas}}(r)$ are the gas temperature and number density, respectively, and $\mu = 0.585$ denotes the mean molecular weight. If the spatial distribution of intracluster gas is described by the conventional β model, $n_{\text{gas}}(r) = n_{\text{gas}}(0)(1 + r^2/r_c^2)^{-3\beta/2}$ where r_c is the core radius of the X-ray gas profile, we can easily get the dynamical mass distribution from equation (2). In order to compare with the gravitational lensing result, we use the projected X-ray cluster mass within radius r (Wu 1994)

$$m_{\text{xray}} = 1.13 \times 10^{13} \beta_{\text{fit}} \tilde{m}(r) \left(\frac{r_c}{0.1 \text{ Mpc}} \right) \left(\frac{kT}{1 \text{ keV}} \right) M_{\odot}, \quad (3)$$

where

$$\tilde{m}(r) = \frac{(R/r_c)^3}{(R/r_c)^2 + 1} - \int_{r/r_c}^{R/r_c} x \sqrt{x^2 - (r/r_c)^2} \frac{3+x^2}{(1+x^2)^2} dx,$$

and R is the physical radius of the cluster and will be taken to be $R = 3$ Mpc in the actual computation. Our conclusion is unaffected by this choice.

2.3 The universal density profile

The virialized dark matter halo follows (NFW)

$$\rho = \frac{\rho_s}{(r/r_s)(1 + r/r_s)^2}, \quad (4)$$

where ρ_s and r_s are the characteristic density and length, respectively. The projected cluster mass within radius r from equation (4) is simply

$$m_{\text{uni}} = \begin{cases} 4\pi \rho_s r_s^3 \cdot \ln \frac{r}{2r_s} + \frac{r_s}{\sqrt{r_s^2 - r^2}} \ln \frac{r_s + \sqrt{r_s^2 - r^2}}{r}, & r < r_s; \\ \ln \frac{r}{2r_s} + \frac{r_s}{\sqrt{r^2 - r_s^2}} \arctan \frac{\sqrt{r^2 - r_s^2}}{r_s}, & r > r_s. \end{cases} \quad (5)$$

In principle, the two parameters ρ_s and r_s can be determined from the observed X-ray surface brightness of intracluster gas or the surface number density of galaxies, in combination with the measurement of X-ray temperature or velocity dispersion of galaxies. We will work with the X-ray data in this paper.

Inserting the total mass $M(r)$ deduced from the NFW profile into equation (2) will result in an analytic form of gas profile (Makino et al. 1998):

$$n_{\text{gas}}(x) = n_{\text{gas}}(0)e^{-\alpha}(1+x)^{\alpha/x}, \quad (6)$$

in which $x = r/r_s$ and $\alpha = 4\pi G \mu m_p \rho_s r_s^2 / kT$. Since $n_{\text{gas}}(\infty) = n_{\text{gas}}(0)e^{-\alpha}$, we introduce a background subtracted gas number density $\tilde{n}(x) = n_{\text{gas}}(x) - n_{\text{gas}}(\infty)$, which reads

$$\tilde{n}(x) = \frac{\tilde{n}(0)}{e^{\alpha} - 1} [(1+x)^{\alpha/x} - 1]. \quad (7)$$

This avoids the divergence in the computation of X-ray surface brightness below. Recall that an arbitrary cut-off radius was used by Makino & Asano (1999) for the same purpose. The X-ray surface brightness in the scenario of the optically thin and isothermal plasma emission is

$$S_x(\theta) \propto \int_{D_d \theta / r_s}^{\infty} \frac{\tilde{n}^2(x) x dx}{\sqrt{x^2 - D_d \theta / r_s}}, \quad (8)$$

A straightforward computation yields

$$S_x(\theta) \propto \int_{\theta/\theta_s}^{\infty} \frac{\sqrt{x^2 - (\theta/\theta_s)^2}}{x} (1+x)^{\alpha/x} \cdot [(1+x)^{\alpha/x} - 1] \left[\frac{1}{1+x} - \frac{\ln(1+x)}{x} \right] dx, \quad (9)$$

in which $\theta_s = r_s/D_d$. Our task is thus reduced to finding out the two parameters α and r_s from the observed X-ray surface brightness S_x and gas temperatures T of clusters, and then to obtain the projected cluster masses from equation (5).

3 CLUSTER SAMPLE AND RESULTS

21 clusters (Table 1) are selected from the Strong Lensing Cluster Sample of Wu et al. (1998) by requiring that both the X-ray temperature and the surface brightness profiles are well measured with *ROSAT* and/or *ASCA*. We have not included those clusters whose temperatures are estimated by indirect methods such as the X-ray luminosity-temperature correlation and the velocity dispersion-temperature correlation. These 21 clusters have a mean redshift of $\langle z_d \rangle = 0.30$, and contain 26 arc-like images. For the 11 arcs that have no redshift information, we estimate their lensing masses m_{lens} by assuming the mean redshifts of $\langle z_s \rangle = 0.8$ and 2.0, respectively. We calculate the values of $m_{\text{lens}}(< r_{\text{arc}})$ for two cosmological models: (1) $\Omega_M = 1$ and $\Omega_{\Lambda} = 0$ and (2) $\Omega_M = 0.3$ and $\Omega_{\Lambda} = 0.7$. The resultant cluster masses enclosed within the positions of 26 arc-like images are listed in Table 1. We have not provided the uncertainties in m_{lens} no matter whether they are derived from the detailed modeling of arcs or from the simple spherical assumption. In principle, there will be no uncertainties associated with m_{lens} in the simple spherical lensing model if redshifts of the lensing clusters and of the arc-like images are reliably determined. However, the presence of substructures and asymmetrical mass distributions in clusters may complicate this simple

cluster mass estimate, which will be the major source of uncertainties in m_{lens} . The absence of the secondary arc-like images in most of the arc-cluster systems should be a strong argument against the spherical mass distribution in the central regions of clusters.

The X-ray surface brightness profiles S_x for our 21 clusters are available in archive (*ROSAT* and *ASCA*), which have been analysed by a number of authors for different purposes. Because the accuracy of our determination of the dynamical cluster mass from X-ray measurement is closely connected to the issue as to how precisely we can describe the observed X-ray surface brightness S_x , two conventional methods are employed in the fitting of S_x (e.g. Neumann & Arnaud 1999): (1) a β model fit to the entire X-ray surface brightness; (2) a β model fit by excising the central region until an improvement of χ^2 can be achieved. The latter is usually applied to the cooling-flow cluster where a sharp peak is seen in the X-ray emission concentrated in the core of the cluster. In Table 2 we list the best-fitting parameters β and r_c from the first fitting method, while the results obtained from the second method are presented in Table 3 for 14 clusters where available in literature. Here we make no attempt as far as possible to extrapolate the original work. For all the clusters we take the temperature data from the literature (see Wu, Xue & Fang 1999; and references therein). In order to explicitly demonstrate the possible effect of cooling/non-cooling flows on the mass ratios of $m_{\text{lens}}/m_{\text{xray}}$, the sample is classified into the massive cooling-flow (MC) clusters, the intermediate cooling-flow (IC) clusters and non-cooling flow (NC) clusters in terms of their cooling times (see Allen 1998). Roughly speaking, the MC, IC and NC clusters in our sample have average mass deposition rates of $\gtrsim 1000M_\odot \text{ yr}^{-1}$, $\sim 100M_\odot \text{ yr}^{-1}$ and $\lesssim 10M_\odot \text{ yr}^{-1}$, respectively. The projected dynamical masses (m_{xray}) of clusters within the arc positions are computed according to equation (3). Finally, the mass ratio of m_{lens} to m_{xray} is obtained for each case and listed in Tables 2 and 3, in which the error bars reflect the combined measurement uncertainties of T , r_c and β .

In principle, we can get the two parameters α (or ρ_s) and r_s in the NFW profile by fitting the observed S_x to the predicted form of equation (9) for all the cases. However, the actual operation turns out to be difficult for some clusters owing to the instrumental PSF of the X-ray telescopes (*ASCA*, *ROSAT*). So, for eight clusters in our sample we estimate the parameters α and r_s using the empirical formula (Ettori & Fabian 1999), $\alpha = 14.34\beta$ and $r_s = 3.17r_c$. For the three clusters (A2219, MS1358 and MS2137), we take the best-fitting values from Ettori & Fabian (1999) who have excluded the cooling-flow regions in their fitting. For the rest clusters, we adopt the results of Wu & Xue (2000), which are obtained by the χ^2 fit of the entire data points of S_x from the Mohr, Mathiesen & Evard (1999) sample to the theoretical predictions (equation 9). The parameters, α and r_s , for all the clusters of our sample are listed in Table 4, together with the derived cluster masses within the positions of arcs and their ratios to the corresponding masses

from strong lensing for a cosmological model of $\Omega_M = 1$ and $\Omega_\Lambda = 0$.

We first compare in Fig.1 the projected cluster masses within arc-like images determined from strong lensing and X-ray measurements, using the data in Table 2, where the values of m_{lens} for $z_s = 2$ are chosen if redshifts of the arcs remain unknown. It appears that the ratios of m_{lens} to m_{xray} display rather large dispersions for many clusters, which is mainly due to the fact that the X-ray surface brightness profiles of these clusters (e.g. A370, CL0500, etc.) have not been well constrained. Yet, the mass ratios of all the data points essentially satisfy $m_{\text{lens}}/m_{\text{xray}} < 2$ when their uncertainties are taken into account. Namely, the lensing and X-ray determined cluster masses are still consistent with each other within a factor of 2, and there is no large discrepancy between these two mass estimates. Additionally, all the clusters which exhibit a relatively large mass ratio of $m_{\text{lens}}/m_{\text{xray}} > 2$, if the error bars are neglected for the moment, are the NC or IC clusters, in contrast with the MS clusters whose mass ratios $m_{\text{lens}}/m_{\text{xray}}$ are roughly consistent with unity. We have thus confirmed the results of Allen (1998). Alternatively, the introduction of a non-zero cosmological constant does help to reduce, though moderately, the mass discrepancy between m_{lens} and m_{xray} .

Next we demonstrate how our X-ray mass measurements within r_{arc} are affected by the two different fittings of the X-ray surface brightness profiles: whether or not the excess X-ray emission in the central cores is excluded. We display in Fig.2 the projected X-ray masses within 17 arc-like images obtained from these two methods for a cosmological model of $\Omega_M = 1$ and $\Omega_\Lambda = 0$. It is immediate that these two methods provide essentially a consistent cluster mass at the central core. Consequently, the mass ratios $m_{\text{lens}}/m_{\text{xray}}$ will remain approximately the same as those in Table 2. even if the goodness of a β model fit is improved by omitting some data points of S_x in the central regions.

Finally, we compare the projected cluster masses within arc-like images derived from the strong lensing, the X-ray measurement based on a β model and the NFW profile. Fig.3 shows the results of $m_{\text{NFW}}(< r_{\text{arc}})$ versus $m_{\text{xray}}(< r_{\text{arc}})$ for our sample of 26 arcs among 21 clusters. Regardless of the large error bars, the cluster masses given by the NFW profile are in good agreement with the values from the X-ray analysis. Indeed, this result contrasts with our initial yet naive speculation that the cusped NFW profile at the cluster center can give rise to a very different cluster mass enclosed within the arc-like image. On the other hand, such a situation is not surprising because both the X-ray and NFW cluster mass estimates are based on the measurements of X-ray surface brightness profiles of clusters and the assumption that the X-ray emitting gas is isothermal and in hydrostatic equilibrium with the underlying gravitational potential of the clusters. Recall that the NFW profile can almost recover the conventional β model for the observed X-ray surface brightness profiles of clusters. This explains the good agreement between these two mass estimates. The similar result has been reported by Lewis et al (1999) if the surface number density of galaxies and their velocity dispersion, instead of the X-ray surface brightness profile of intracluster gas and its temperature, are used to calibrate the NFW profile. As a result, the cusped NFW profile is of no help to resolving the mass discrepancy between the strong lensing and X-ray

Table 1. Strong Lensing Cluster Sample

cluster	z_{cluster}	z_{arc}	r_{arc} (Mpc)		$m_{\text{lens}}(10^{14}M_{\odot})$	
			$\Omega_M = 1$	$\Omega_M = 0.3$	$\Omega_M = 1$	$\Omega_M = 0.3$
A370 ⁺	0.373	1.3	0.35	0.41	13.0	13.6
		0.724	0.16	0.19	2.90	2.99
A963 ⁺	0.206	...	0.0517	0.0567	0.25(0.21)*	0.25(0.21)*
		0.711	0.080	0.088	0.60	0.61
A1689	0.181	...	0.183	0.199	3.6(3.0)*	3.7(3.2)*
A1835	0.252	...	0.150	0.167	1.98(1.54)*	2.02(1.60)*
A2163	0.203	0.728	0.0661	0.0724	0.41	0.42
A2218 ⁺	0.171	1.034	0.26	0.28	2.70	2.75
		0.702	0.0794	0.0859	0.623	0.632
		2.515	0.0848	0.091	0.570	0.587
A2219 ⁺	0.228	...	0.079	0.087	0.517(0.415)*	0.527(0.429)*
		...	0.110	0.122	1.60(1.28)*	1.63(1.32)*
A2390	0.228	0.913	0.177	0.196	2.54	2.60
CL0024	0.391	1.675	0.220	0.257	2.6	2.7
CL0500	0.327	...	0.15	0.17	1.90(1.33)*	1.95(1.39)*
CL2236	0.552	1.116	0.0876	0.107	0.30	0.32
CL2244	0.328	2.236	0.0465	0.0532	0.20	0.21
MS0302	0.423	...	0.122	0.144	1.60(0.95)*	1.66(1.01)*
MS0440	0.197	0.530	0.089	0.097	0.89	0.90
MS0451	0.539	...	0.190	0.230	5.2(2.3)*	5.4(2.4)*
MS1008	0.306	...	0.26	0.30	6.1(4.4)*	6.3(4.6)*
MS1358	0.329	4.92	0.121	0.139	0.827	0.882
MS1455	0.257	...	0.098	0.110	0.86(0.67)*	0.88(0.69)*
MS2137	0.313	...	0.0874	0.0995	0.71(0.51)*	0.73(0.53)*
PKS0745	0.103	0.433	0.0459	0.0482	0.30	0.30
RXJ1347	0.451	0.81	0.24	0.28	4.2	4.4

⁺Multiple-arc system.

*Arc-like image is assumed at $z_s = 0.8$ ($z_s = 2$).

Table 2. X-ray properties: a standard β fit to the entire X-ray surface brightness

PLEASE PLACE TABLE 2 HERE

measurements, and the ratios of $m_{\text{lens}}/m_{\text{NFW}}$ listed in Table 4 remain roughly the same as the values of $m_{\text{lens}}/m_{\text{xray}}$ in Table 2. If there are any differences between the NFW and X-ray mass estimates, they are certainly beyond the regions accessible to current lensing and X-ray data. It could be misleading if one simply extrapolates our present mass comparison into smaller (or larger) radii.

4 DISCUSSION AND CONCLUSIONS

We have conducted a combined analysis of the cluster mass estimates from the strong lensing, the X-ray measurement and the NFW profile, aiming at reducing the mass discrepancy between the strong lensing and X-ray measurements reported in literature (see Wu & Fang 1997). In particular, the cusped NFW profile at the central regions of clusters was thought to be promising for providing a new insight into the

problem. Basically, these three mass estimates originated from very different motivations, and should in principle be independent of each other. However, the actual application of the NFW profile needs the priori calibration of the two free parameters, ρ_s and r_s , which requires the knowledge about the baryonic mass distributions (galaxies and intra-cluster gas) in clusters, in conjunction with the spectroscopic measurements of the velocity dispersion/temperature of the clusters. So, when the X-ray data are used to fix the NFW profile, there is a common working hypothesis behind the X-ray and NFW mass estimates: i.e., the hydrostatic equilibrium and isothermality for the intracluster gas. Therefore, the gravitational lensing appears to be the unique mass estimate at present independently of the dynamical state of clusters.

From a detailed comparison of the projected cluster masses enclosed within 26 arc-like images among 21 clusters

Table 3. X-ray properties: cooling flow regions excluded

PLEASE PLACE TABLE 3 HERE

Table 4. Cluster properties: the NFW profile

cluster	α	r_s (Mpc)	$m_{\text{NFW}} (< r_{\text{arc}})^*$	$m_{\text{lens}}/m_{\text{NFW}}$
A370	$13.62^{+10.76}_{-5.02}$ (3)	$1.52^{+1.20}_{-0.70}$ (3)	$2.57^{+19.89}_{-2.27}$ $0.77^{+6.58}_{-0.15}$	$5.05^{+37.20}_{-4.47}$ $3.78^{+29.98}_{-3.38}$
A963	$7.31^{+0.57}_{-0.57}$ (3)	$0.31^{+0.07}_{-0.07}$ (3)	$0.15^{+0.15}_{-0.07}$ $0.29^{+0.28}_{-0.14}$	$1.68^{+3.32}_{-0.85}$ $2.10^{+1.96}_{-1.04}$
A1689	$10.93^{+0.44}_{-0.44}$ (1)	$0.72^{+0.07}_{-0.07}$ (1)	$1.44^{+0.58}_{-0.40}$	$2.51^{+0.98}_{-0.72}$
A1835	$9.00^{+0.69}_{-0.69}$ (1)	$0.23^{+0.05}_{-0.05}$ (1)	$1.44^{+1.51}_{-0.76}$	$1.37^{+1.52}_{-0.70}$
A2163	$8.83^{+0.16}_{-0.16}$ (1)	$1.03^{+0.06}_{-0.06}$ (1)	$0.31^{+0.08}_{-0.06}$	$1.34^{+0.36}_{-0.28}$
A2218	$9.19^{+0.33}_{-0.33}$ (1)	$0.88^{+0.08}_{-0.08}$ (1)	$1.44^{+0.49}_{-0.36}$ $0.23^{+0.09}_{-0.07}$ $0.26^{+0.09}_{-0.07}$	$1.87^{+0.63}_{-0.47}$ $2.67^{+0.97}_{-0.71}$ $2.19^{+0.79}_{-0.59}$
A2219	11.51(2)	1.59(2)	$0.34^{+0.01}_{-0.01}$ $0.59^{+0.02}_{-0.02}$	$1.51^{+0.06}_{-0.06}$ $2.69^{+0.11}_{-0.10}$
A2390	$8.76^{+0.23}_{-0.23}$ (1)	$0.54^{+0.03}_{-0.03}$ (1)	$1.52^{+0.45}_{-0.36}$	$1.67^{+0.51}_{-0.38}$
CL0024	$6.81^{+1.08}_{-0.72}$ (3)	$0.21^{+0.12}_{-0.08}$ (3)	$1.00^{+4.52}_{-0.80}$	$2.59^{+9.96}_{-2.12}$
CL0500	$12.91^{+7.17}_{-4.3}$ (3)	$1.30^{+0.67}_{-0.76}$ (3)	$0.73^{+9.16}_{-0.65}$	$2.61^{+22.01}_{-2.42}$
CL2236	$7.60^{+2.58}_{-1.29}$ (3)	$0.21^{+0.13}_{-0.09}$ (3)	$0.40^{+2.00}_{-0.33}$	$0.75^{+3.39}_{-0.63}$
CL2244	$3.81^{+0.09}_{-0.09}$ (3)	$0.22^{+0.10}_{-0.10}$ (3)	$0.085^{+0.298}_{-0.064}$	$2.36^{+7.48}_{-1.84}$
MS0302	$7.30^{+1.27}_{-1.27}$ (1)	$0.17^{+0.09}_{-0.09}$ (1)	$0.46^{+1.60}_{-0.36}$	$3.51^{+14.04}_{-2.73}$
MS0440	$5.62^{+0.17}_{-0.17}$ (1)	$0.075^{+0.011}_{-0.011}$ (1)	$0.31^{+0.22}_{-0.12}$	$2.84^{+1.85}_{-1.18}$
MS0451	$5.32^{+0.56}_{-0.56}$ (1)	$0.44^{+0.14}_{-0.14}$ (1)	$1.01^{+1.69}_{-0.63}$	$5.17^{+3.33}_{-3.24}$
MS1008	$9.03^{+1.58}_{-1.00}$ (3)	$0.64^{+0.20}_{-0.15}$ (3)	$1.64^{+3.18}_{-1.03}$	$3.72^{+6.38}_{-2.46}$
MS1358	14.29(2)	1.48(2)	$0.55^{+0.31}_{-0.31}$	$1.51^{+2.03}_{-0.55}$
MS1455	$7.34^{+0.43}_{-0.43}$ (1)	$0.13^{+0.045}_{-0.045}$ (1)	$0.44^{+0.60}_{-0.26}$	$1.96^{+2.75}_{-1.13}$
MS2137	11.48(2)	0.18(2)	$0.45^{+0.04}_{-0.07}$	$1.59^{+0.31}_{-0.13}$
PKS0745	$8.93^{+0.10}_{-0.10}$ (1)	$0.27^{+0.01}_{-0.01}$ (1)	$0.23^{+0.08}_{-0.06}$	$1.29^{+0.44}_{-0.35}$
RXJ1347	$8.17^{+0.57}_{-0.20}$ (3)	$0.18^{+0.01}_{-0.04}$ (3)	$2.64^{+2.07}_{-1.10}$	$1.59^{+1.14}_{-0.70}$

Nores. *In units of $10^{14}M_{\odot}$.

(1)From Wu & Xue (2000).

(2)From Ettori & Fabian (1999).

(3)Estimated from α - β and r_s - r_c relations (Ettori & Fabian 1999).

obtained from the three mass estimates, we have arrived at the following conclusions:

(i)The mass discrepancy among the three methods are actually within a factor of 2, if X-ray measurement uncertainties are included. This is particularly true if a non-zero cosmological constant is invoked.

(ii)We have confirmed the finding by Allen (1999) that the mass ratios of m_{lens} to m_{xray} (or m_{NFW}) are consistent with unity for the massive cooling flow clusters, indicating that they are the more dynamically relaxed systems.

(iii)Our X-ray mass estimates within r_{arc} are little affected by whether or not the excess X-ray emission in the central cores is excluded in the fit of the observed X-ray surface brightness.

(iv)The cluster masses within the arc-like images deter-

mined from the X-ray and NFW methods show an excellent agreement. Any differences between these two methods must occur at even smaller radii ($< r_{\text{arc}}$) or at large radii. This arises because both methods have assumed the isothermality and hydrostatic equilibrium for the intracluster gas. In other words, the employment of the cusped NFW profile for the dark matter distribution of clusters cannot resolve the reported mass discrepancy between the strong lensing and X-ray measurements claimed in literature.

Taking these results as a whole, together with the previous finding that there is good agreement between the X-ray, optical and weak lensing determined cluster masses on scales greater than the X-ray core sizes (Wu & Fang 1997; Allen 1998; Wu et al. 1998), we feel that the reported mass discrepancy in the IC, especially NC clusters is likely to have

arisen from the oversimplification of the modeling of central mass distributions of the clusters as lenses. Indeed, if the presence of cooling flows in the central cores of clusters is a reliable indicator of their dynamical relaxation (Allen 1998), it would not be difficult to understand the reported mass discrepancy in the central regions of the IC and NC clusters where the local dynamical activities play a dominant role in the organization of the central matter distributions. Consequently, a simple spherical lens model may lead to an overestimate of the gravitating masses of the lensing clusters (e.g. Bartelmann & Steinmetz 1996; Allen 1998; Wu et al. 1998; etc.), and meanwhile the X-ray mass estimate including the NFW method should also allow the intracluster gas to deviate from the isothermal and hydrostatic equilibrium distributions.

ACKNOWLEDGMENTS

I would like to thank Simon White for pointing to me this research, and an anonymous referee for valuable comments and suggestions. This work was supported by the National Science Foundation of China, under Grant No. 1972531.

REFERENCES

- Allen S.W., 1998, MNRAS, 296, 392
 Allen S.W., Fabian A.C., Edge A.C., Bautz M.W., Furuzawa A., Tawara Y., 1996, MNRAS, 283, 263
 Arnaud M., Evrard A.E., 1999, MNRAS, 305, 631
 Bartelmann M., Steinmetz M., 1996, MNRAS, 283, 431
 Carlberg R.G., Yee H.K.C., Ellingson E., 1997, ApJ, 478, 462
 Cole S., Lacey C., 1996, MNRAS, 281, 716
 Eke V.R., Navarro J.F., Frenk C.S., 1998, ApJ, 503, 569
 Elbaz D., Arnaud M., Böhringer H., 1995, A&A, 293, 337
 Ettori S., Fabian A.C., 1999, MNRAS, 305, 834
 Gioia I.M., Shaya E.J., Le Fèvre O., Falco E.E., Luppino G.A., Hammer F., 1998, ApJ, 497, 573
 Grossman S.A., Saha P., 1994, ApJ, 431, 74
 Hammer F., 1991, ApJ, 383, 66
 Lewis A.D., Ellingson E., Morris S.L., Carlberg R.G., 1999, ApJ, 517, 587
 Loeb A., Mao S., 1994, ApJ, 435, L109
 Miralda-Escudé J., Babul A., 1995, ApJ, 449, 18
 Makino N., Asano K., 1999, 512, 9
 Makino N., Sasaki S., Suto Y., 1998, ApJ, 497, 55
 Mohr J.J., Mathiesen B., Evrard A.E., 1999, ApJ, 517, 627
 Molikawa K., Hattori M., Kneib J.-P., Yamashita K., 1999, A&A, 351, 418
 Navarro J.F., Frenk C.S., White S.D.M., 1995, MNRAS, 275, 720 (NFW)
 Navarro J.F., Frenk C.S., White S.D.M., 1997, ApJ, 490, 493
 Neumann D.M., Arnaud M., 1999, 348, 711
 Ota N., Mitsuda K., Fukazawa Y., 1998, ApJ, 495, 170
 Rizza E., Burns J.O., Ledlow M.J., Owen F.N., Voges W., Bliton M., 1998, MNRAS, 301, 328
 Schindler S., 1999, A&A, 349, 435
 Soucail G., Ota N., Böhringer H., Czoske O., Hattori M., Mellier Y., 1999, A&A, submitted (astro-ph/9911062)
 Vikhlinin A., Forman W., Jones C., 1999, ApJ, 525, 47
 Wu X.-P., 1994, ApJ, 436, L115
 Wu X.-P., Chiueh T., Fang L.-Z., Xue Y.-J., 1998, MNRAS, 301, 861
 Wu X.-P., Fang L.-Z., 1997, ApJ, 483, 62
 Wu X.-P., Hammer F., 1993, MNRAS, 262, 187

- Wu X.-P., Xue Y.-J., Fang L.-Z., 1999, ApJ, 524, 22
 Wu X.-P., Xue Y.-J., 2000, ApJ, 529, L5

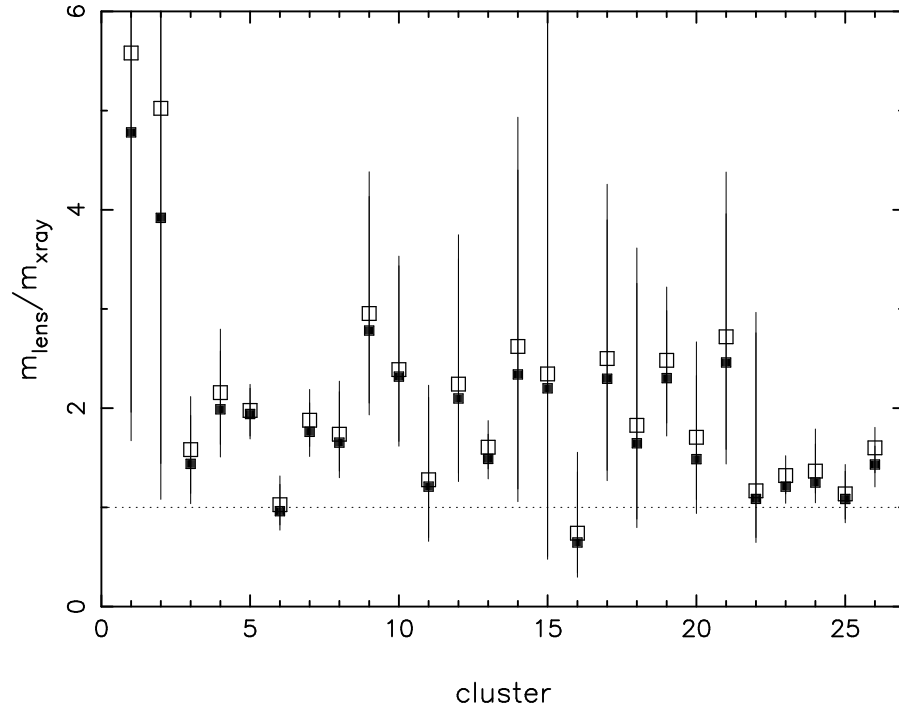


Figure 1. Ratios of the strong lensing and X-ray determined cluster masses enclosed within 26 arc-like images among 21 clusters. The horizontal axis is ordered in terms of the arc list in Table 1. A flat cosmological model with ($\Omega_{\Lambda} = 0.7$, filled squares) and without ($\Omega_{\Lambda} = 0$, open squares) the cosmological constant is used. For the 11 arc-like images whose redshifts are not available, we adopt a mean value of $z_s = 2$.

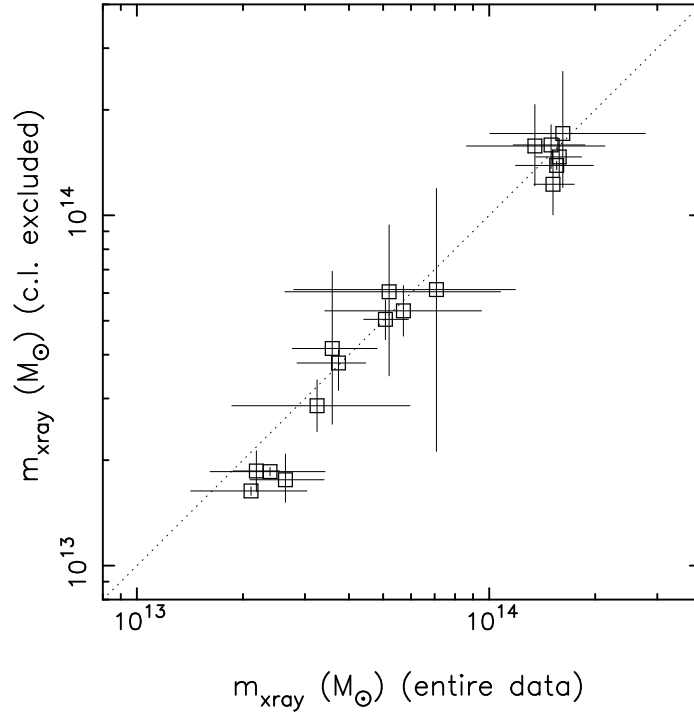


Figure 2. A comparison of the X-ray cluster masses enclosed within 17 arc-like images among 14 clusters (Table 3) derived from two different fittings of the X-ray surface brightness S_x of the clusters: (1) a β model fitted to the entire S_x (horizontal axis), and (2) a β model fit by excising the central region of S_x until an acceptable χ^2 is achieved (vertical axis). A flat cosmological model of $\Omega_M = 1$ is assumed.

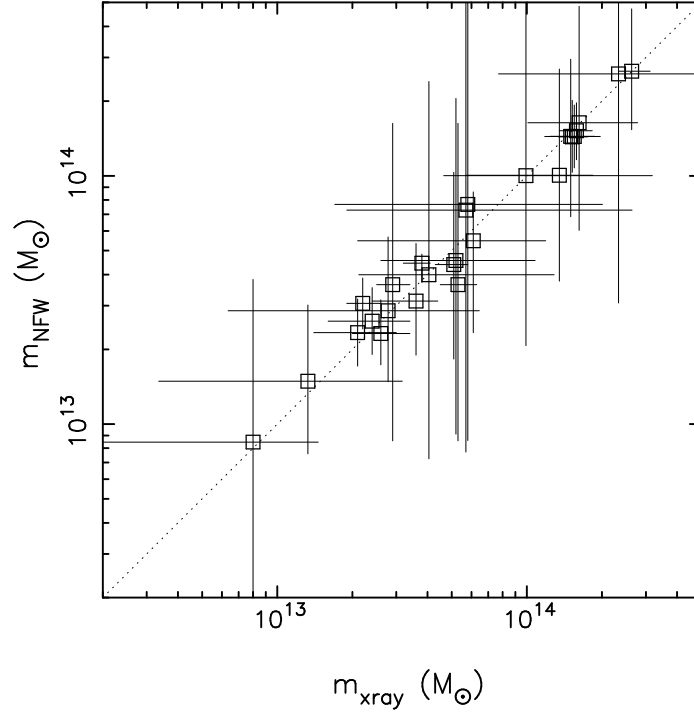


Figure 3. The NFW profile derived cluster masses m_{NFW} within 26 arc-like images are plotted against the corresponding X-ray masses (m_{xray}). Data are taken from Table 4.

Table 2: X-ray properties: a standard β fit to the entire X-ray surface brightness profile

cluster	T (keV)	β	ref ^d	$\Omega_M = 1$				$\Omega_M =$
				r_c (Mpc)	m_{xray}^b	m_{lens}/m_{xray}	r_c (Mpc)	m_{xray}^b
A370	$7.13^{+1.05}_{-1.05}$	$0.95^{+0.75}_{-0.35}$	1	$0.48^{+0.38}_{-0.22}$	$2.33^{+4.30}_{-1.56}$	$5.58^{+11.29}_{-3.62}$	$0.56^{+0.44}_{-0.26}$	$2.85^{+5.29}_{-1.92}$
A963	$6.13^{+0.45}_{-0.30}$	$0.51^{+0.04}_{-0.04}$	2	$0.098^{+0.021}_{-0.021}$	$0.58^{+1.43}_{-0.41}$	$5.02^{+11.83}_{-3.58}$	$0.107^{+0.023}_{-0.023}$	$0.74^{+1.94}_{-0.53}$
A1689	$9.02^{+0.40}_{-0.30}$	$0.65^{+0.04}_{-0.02}$	3	$0.131^{+0.022}_{-0.014}$	$0.13^{+0.05}_{-0.03}$	$1.88^{+0.64}_{-0.53}$	$(1.58^{+0.53}_{-0.44})^c$	$0.15^{+0.06}_{-0.04}$
A1835	$9.8^{+1.4}_{-1.4}$	$0.65^{+0.04}_{-0.04}$	4	$0.074^{+0.011}_{-0.011}$	$0.28^{+0.09}_{-0.06}$	$2.16^{+0.64}_{-0.52}$	$(1.98^{+0.26}_{-0.26})^c$	$0.31^{+0.10}_{-0.07}$
A2163	$14.6^{+0.85}_{-0.85}$	$0.62^{+0.02}_{-0.02}$	5	$0.305^{+0.019}_{-0.019}$	$1.52^{+0.23}_{-0.18}$	$2.37^{+0.32}_{-0.31}$	$(1.03^{+0.29}_{-0.20})^c$	$1.65^{+0.25}_{-0.19}$
A2218	$7.1^{+0.2}_{-0.2}$	$0.65^{+0.08}_{-0.05}$	5	$0.226^{+0.080}_{-0.050}$	$1.50^{+0.37}_{-0.33}$	$1.32^{+0.37}_{-0.26}$	$(1.03^{+0.29}_{-0.20})^c$	$1.66^{+0.41}_{-0.37}$
A2219	$12.4^{+0.5}_{-0.5}$	$0.40^{+0.07}_{-0.07}$	2	$0.147^{+0.068}_{-0.068}$	$0.22^{+0.04}_{-0.03}$	$1.88^{+0.31}_{-0.26}$	$0.334^{+0.021}_{-0.021}$	$0.24^{+0.04}_{-0.03}$
A2390	$11.1^{+1.0}_{-1.0}$	$0.59^{+0.02}_{-0.02}$	6	$0.140^{+0.009}_{-0.009}$	$1.55^{+0.42}_{-0.37}$	$1.74^{+0.53}_{-0.37}$	$0.245^{+0.087}_{-0.054}$	$1.66^{+0.45}_{-0.39}$
CL0024	$5.7^{+4.9}_{-2.1}$	$0.475^{+0.075}_{-0.050}$	7	$0.066^{+0.039}_{-0.025}$	$0.21^{+0.09}_{-0.07}$	$2.95^{+1.43}_{-0.90}$	$0.23^{+0.10}_{-0.07}$	$0.25^{+0.11}_{-0.08}$
CL0500	$7.2^{+3.7}_{-1.8}$	$0.9^{+0.5}_{-0.3}$	1	$0.41^{+0.21}_{-0.24}$	$0.33^{+0.27}_{-0.14}$	$1.59^{+1.19}_{-0.72}$	$(1.28^{+0.95}_{-0.58})^c$	$0.163^{+0.075}_{-0.075}$
CL2236	$6.2^{+2.6}_{-1.7}$	$0.53^{+0.18}_{-0.09}$	8	$0.066^{+0.041}_{-0.027}$	$0.57^{+0.38}_{-0.23}$	$2.80^{+1.88}_{-1.12}$	$(2.25^{+1.51}_{-0.91})^c$	$0.36^{+0.30}_{-0.15}$
CL2244	$6.5^{+1.8}_{-1.3}$	$0.266^{+0.006}_{-0.006}$	1	$0.068^{+0.031}_{-0.031}$	$0.24^{+0.10}_{-0.08}$	$2.39^{+1.14}_{-0.72}$	$0.25^{+0.11}_{-0.08}$	$0.63^{+0.42}_{-0.25}$
MS0302	$4.6^{+0.8}_{-0.8}$	$0.62^{+0.34}_{-0.13}$	9	$0.075^{+0.063}_{-0.044}$	$0.33^{+0.27}_{-0.14}$	$1.59^{+1.19}_{-0.72}$	$(1.28^{+0.95}_{-0.58})^c$	$0.36^{+0.30}_{-0.15}$
MS0440	$5.30^{+1.27}_{-0.85}$	$0.45^{+0.03}_{-0.03}$	10	$0.027^{+0.005}_{-0.005}$	$0.57^{+0.38}_{-0.23}$	$2.80^{+1.88}_{-1.12}$	$(2.25^{+1.51}_{-0.91})^c$	$0.63^{+0.42}_{-0.25}$
MS0451	$10.17^{+1.55}_{-1.26}$	$0.68^{+0.13}_{-0.09}$	8	$0.256^{+0.069}_{-0.053}$	$1.58^{+0.25}_{-0.23}$	$1.61^{+0.27}_{-0.22}$	$0.155^{+0.010}_{-0.010}$	$1.75^{+0.27}_{-0.25}$
MS1008	$7.29^{+2.45}_{-1.52}$	$0.63^{+0.11}_{-0.07}$	9	$0.203^{+0.064}_{-0.048}$	$0.99^{+1.20}_{-0.46}$	$2.62^{+2.31}_{-1.44}$	$0.077^{+0.045}_{-0.029}$	$1.15^{+1.40}_{-0.54}$
MS1358	$7.5^{+4.3}_{-4.3}$	$0.47^{+0.02}_{-0.02}$	9	$0.042^{+0.013}_{-0.009}$	$0.57^{+2.07}_{-0.38}$	$3.35^{+6.67}_{-2.63}$	$(2.34^{+4.67}_{-1.84})^c$	$0.47^{+0.24}_{-0.27}$
MS1455	$5.45^{+0.29}_{-0.28}$	$0.64^{+0.04}_{-0.03}$	9	$0.062^{+0.009}_{-0.008}$	$0.41^{+0.48}_{-0.21}$	$0.74^{+0.82}_{-0.40}$	$0.080^{+0.050}_{-0.033}$	$0.50^{+0.58}_{-0.26}$
MS2137	$4.37^{+0.38}_{-0.72}$	$0.63^{+0.04}_{-0.03}$	9	$0.047^{+0.008}_{-0.007}$	$0.080^{+0.066}_{-0.033}$	$2.50^{+1.76}_{-1.13}$	$0.078^{+0.035}_{-0.035}$	$0.091^{+0.074}_{-0.038}$
PKS0745	$8.7^{+1.6}_{-1.2}$	$0.59^{+0.01}_{-0.01}$	3	$0.056^{+0.006}_{-0.006}$	$0.52^{+0.56}_{-0.26}$	$3.08^{+3.01}_{-1.59}$	$(1.83^{+1.79}_{-0.95})^c$	$0.61^{+0.65}_{-0.30}$
RXJ1347	$11.37^{+1.10}_{-0.92}$	$0.57^{+0.04}_{-0.014}$	8	$0.057^{+0.012}_{-0.012}$	$0.36^{+0.12}_{-0.08}$	$2.48^{+0.74}_{-0.63}$	$0.029^{+0.005}_{-0.005}$	$0.39^{+0.13}_{-0.09}$
					$1.35^{+0.78}_{-0.49}$	$3.86^{+2.17}_{-1.42}$	$(1.71^{+0.96}_{-0.63})^c$	$0.311^{+0.084}_{-0.064}$
					$1.62^{+1.16}_{-0.61}$	$3.77^{+2.30}_{-1.57}$	$(2.72^{+1.66}_{-1.13})^c$	$0.230^{+0.073}_{-0.054}$
					$0.71^{+0.48}_{-0.43}$	$1.17^{+1.80}_{-0.47}$	$0.048^{+0.015}_{-0.011}$	$0.81^{+0.55}_{-0.49}$
					$0.51^{+0.08}_{-0.07}$	$1.70^{+0.26}_{-0.24}$	$(1.32^{+0.20}_{-0.18})^c$	$0.069^{+0.010}_{-0.009}$
					$0.37^{+0.07}_{-0.09}$	$1.90^{+0.59}_{-0.31}$	$(1.37^{+0.42}_{-0.22})^c$	$0.054^{+0.009}_{-0.008}$
					$0.26^{+0.08}_{-0.06}$	$1.14^{+0.30}_{-0.25}$	$0.059^{+0.006}_{-0.006}$	$0.28^{+0.08}_{-0.10}$
					$2.63^{+0.49}_{-0.30}$	$1.60^{+0.21}_{-0.25}$	$0.068^{+0.014}_{-0.014}$	$3.04^{+0.57}_{-0.35}$

^aMC: massive cooling-flow; IC: intermediate cooling-flow; NC: non-cooling flow; U: Unclear.

^bIn units of $10^{14}M_{\odot}$.

^cArc-like image is assumed at $z_s = 0.8$ ($z_s = 2$).

^dReferences: (1)Ota, Mitsuda & Fukazawa (1998); (2)Rizza et al. (1998); (3)Mohr, Mathiesen & Evrard (1999); (4)Allen (1998); (5)Arnaud & Evrard (1999); (6)Elbaz et al. (1995); (7)Soucail et al. (1999); (8)Schindler (1999); (9)Molikawa et al. (1999).

Table 3: X-ray properties: cooling-flow regions excluded

cluster	T (keV)	β	ref ^c	$\Omega_M = 1$				$\Omega_M = 0.3$
				r_c (Mpc)	m_{xray}^a	m_{lens}/m_{xray}	r_c (Mpc)	m_{xray}^a
A1689	$9.02^{+0.40}_{-0.30}$	$0.77^{+0.03}_{-0.03}$	1	$0.27^{+0.05}_{-0.05}$	$1.23^{+0.30}_{-0.22}$	$2.94^{+0.65}_{-0.57}$ ($2.45^{+0.54}_{-0.48}$) ^b	$0.29^{+0.05}_{-0.05}$	$1.34^{+0.31}_{-0.23}$
A1835	$9.8^{+1.4}_{-1.4}$	0.72	2	0.09	$1.59^{+0.23}_{-0.23}$	$1.25^{+0.21}_{-0.16}$ ($0.97^{+0.16}_{-0.12}$) ^b	0.10	$1.76^{+0.25}_{-0.25}$
A2163	$14.6^{+0.85}_{-0.85}$	$0.73^{+0.02}_{-0.02}$	1	$0.42^{+0.02}_{-0.02}$	$0.19^{+0.03}_{-0.02}$	$2.20^{+0.32}_{-0.27}$	$0.46^{+0.02}_{-0.02}$	$0.20^{+0.03}_{-0.03}$
A2218	$7.1^{+0.2}_{-0.2}$	0.70	2	0.30	$1.39^{+0.04}_{-0.04}$	$1.95^{+0.06}_{-0.05}$	0.32	$1.56^{+0.04}_{-0.04}$
A2219	$12.4^{+0.5}_{-0.5}$	$0.75^{+0.04}_{-0.04}$	3	$0.339^{+0.026}_{-0.026}$	$0.16^{+0.01}_{-0.01}$ $0.19^{+0.01}_{-0.01}$	$3.81^{+0.11}_{-0.10}$ $3.07^{+0.09}_{-0.08}$	$0.375^{+0.029}_{-0.029}$	$0.19^{+0.01}_{-0.01}$ $0.21^{+0.01}_{-0.01}$
A2390	$11.1^{+1.0}_{-1.0}$	$0.62^{+0.01}_{-0.01}$	4	$0.183^{+0.007}_{-0.007}$	$0.29^{+0.05}_{-0.04}$	$1.81^{+0.33}_{-0.28}$ ($1.45^{+0.27}_{-0.23}$) ^b	$0.375^{+0.029}_{-0.029}$	$0.31^{+0.06}_{-0.05}$
MS0302	$4.6^{+0.8}_{-0.8}$	$0.68^{+0.15}_{-0.15}$	4	$0.058^{+0.031}_{-0.031}$	$0.53^{+0.10}_{-0.08}$	$3.00^{+0.54}_{-0.46}$ ($2.42^{+0.42}_{-0.39}$) ^b		$0.59^{+0.11}_{-0.09}$
MS0440	$5.30^{+1.27}_{-0.85}$	$0.68^{+0.10}_{-0.10}$	4	$0.081^{+0.029}_{-0.029}$	$1.47^{+0.19}_{-0.18}$	$1.73^{+0.24}_{-0.20}$	$0.202^{+0.008}_{-0.008}$	$1.62^{+0.21}_{-0.20}$
MS0451	$10.17^{+1.55}_{-1.26}$	$0.84^{+0.06}_{-0.06}$	4	$0.277^{+0.022}_{-0.024}$	$0.61^{+0.33}_{-0.26}$	$2.64^{+1.95}_{-0.94}$	$0.068^{+0.036}_{-0.036}$	$0.71^{+0.39}_{-0.30}$
MS1008	$7.29^{+2.45}_{-1.52}$	$0.68^{+0.05}_{-0.05}$	4	$0.213^{+0.024}_{-0.024}$	$0.42^{+0.28}_{-0.16}$	$2.13^{+1.38}_{-0.85}$	$0.089^{+0.032}_{-0.032}$	$0.45^{+0.30}_{-0.18}$
MS1358	$7.5^{+4.3}_{-4.3}$	$0.83^{+0.11}_{-0.10}$	4	$0.227^{+0.024}_{-0.024}$	$1.58^{+0.49}_{-0.36}$	$3.30^{+0.99}_{-0.79}$ ($1.46^{+0.44}_{-0.35}$) ^b	$0.336^{+0.027}_{-0.029}$	$1.89^{+0.59}_{-0.44}$
MS1455	$5.45^{+0.29}_{-0.28}$	$0.66^{+0.03}_{-0.03}$	4	$0.070^{+0.007}_{-0.007}$	$1.71^{+0.86}_{-0.51}$	$3.56^{+1.52}_{-1.19}$ ($2.57^{+1.10}_{-0.86}$) ^b	$0.242^{+0.027}_{-0.027}$	$1.98^{+0.99}_{-0.59}$
MS2137	$4.37^{+0.38}_{-0.72}$	0.81	2	0.09	$0.61^{+0.58}_{-0.40}$	$1.35^{+2.55}_{-0.65}$	$0.260^{+0.027}_{-0.027}$	$0.70^{+0.66}_{-0.46}$
PKS0745	$8.7^{+1.6}_{-1.2}$	0.65	2	0.11	$0.51^{+0.07}_{-0.06}$	$1.70^{+0.24}_{-0.20}$ ($1.33^{+0.19}_{-0.16}$) ^b	$0.078^{+0.008}_{-0.008}$	$0.57^{+0.08}_{-0.07}$
					$0.38^{+0.03}_{-0.06}$	$1.87^{+0.37}_{-0.15}$ ($1.35^{+0.27}_{-0.11}$) ^b	0.10	$0.44^{+0.04}_{-0.07}$
					$0.18^{+0.03}_{-0.02}$	$1.71^{+0.27}_{-0.26}$	0.12	$0.18^{+0.03}_{-0.03}$

^aIn units of $10^{14}M_{\odot}$.^bArc-like image is assumed at $z_s = 0.8$ ($z_s = 2$).^cReferences: (1)Vikhlinin, Forman & Jones (1999); (2)Ettori & Fabian (1999); (3)Rizza et al. (1998); (4)Lewis et al.